

CHAPTER 113

Phase-Locking of Modes in the Nearshore: Field Evidence

J. W. Haines*

A. J. Bowen*

Field investigations have shown that infragravity frequencies may dominate nearshore fluid motions (Bowen and Huntley, 1984). Theoretical studies have suggested that the modal structure of the infragravity field, including the degree of modal coupling, is important in generating complicated beach morphologies (Holman and Bowen, 1982) but previous analyses of field data have not provided a description of the infragravity field which is sufficiently detailed to assess the importance of these ideas.

In this paper we present a statistical method which, when applied to data from any large sensor array, provides the desired description of the infragravity field. The method is applied to data from the NSTS (Nearshore Sediment Transport Study) experiment. The variance of the observed velocity field is described by a set of free wave modes. The results indicate that a complicated infragravity field composed of both edge waves and leaky modes is present. The modes modelled are also found to be significantly coupled over a range of modal pairs and frequencies.

Introduction

Results from the analysis of extensive sets of field data have convincingly demonstrated the importance of infragravity motions in the nearshore (Bowen and Huntley, 1984). Observations show that these lower frequency motions may dominate the velocity and elevation fields at the shoreline and across the inner surfzone (Guza and Thornton, 1982). Numerical and analytical models have suggested that these infragravity waves may be important agents of morphologic evolution and may significantly modify the incident wind-wave field. Evaluation of such models requires knowledge of the detailed structure of the infragravity wave field in natural systems.

Bowen and Inman (1971) and Guza and Inman (1975) considered simple models of phase-locked edge waves progressing in opposite directions alongshore. The second-order mean drift velocity and the alongshore variations in shoreline run-up due to these standing edge waves were shown to produce zones of convergence leading to the formation of shoreline cusps and crescentic bars. More complicated infragravity wave fields were modelled by Holman and Bowen (1982). They described the mean drift due to coupled modes of variable mode number and direction of propagation. The resulting time-averaged velocity field varied both across and along the beach, providing a mechanism for the generation of complicated topography varying alongshore on a variety of scales.

These theoretical studies suggest that the coupling or phase-locking of infragravity modes is necessary for the generation of three-dimensional topography. Field evidence for the existence of coupled modes is scarce. Holman and Bowen (1984) showed that standing edge waves were present on a beach bounded by reflective headlands. More complete descriptions of the infragravity field, utilizing large sensor arrays, have failed to address the possible coupling of modes. In this paper we shall describe a new method of describing a large data set in terms of prescribed modes (Haines, et al., in prep.). The method returns

* Department of Oceanography, Dalhousie University, Halifax, NS B3H 4J1 Canada

the time-averaged modal amplitudes, the degree of modal coupling and the relative phase between modes. The resulting detailed picture of the infragravity wave field should provide constraints for physical models of infragravity wave generation, interaction and decay.

Theory and Background

A variety of motions in the nearshore zone are driven by the flux of momentum due to wind-generated waves incident on the beach. The response to this forcing is spread across a broad band of frequencies. The higher frequencies, harmonics of the incident waves and turbulence at the boundaries may stir up and transport the underlying sediment. Larger scale spatially coherent responses to the forcing are predominantly confined to the infragravity frequencies; i.e. those frequencies below the incident wave band. Theoretical investigations have identified a number of possible infragravity responses to various types of forcing.

Both forced and free responses may occur in the nearshore. A broad-banded (in frequency and direction) incident wave field will result in a similarly complicated forcing function. Modification of the incident field due to shoaling and breaking may significantly alter the forcing (Symonds *et al.*, 1982). We are concerned here with the free wave response of the system as described by the linearised shallow-water equations of motion. These solutions include both trapped modes confined to the nearshore and leaky modes which may propagate into and out of the region.

The trapped modes, or edge waves, are a discrete set of modes described by the eigen-solutions of the shallow-water equations (Eckart, 1951). For a planar beach with slope $\tan \beta$ the velocity potential and dispersion relation are given by

$$\Phi_n = \Re \{ g\sigma^{-1} e^{-l_n x} L_n(2l_n x) \alpha_n e^{i(l_n y + \sigma t)} \} \tag{1}$$

and

$$\sigma^2 = gl_n(2n + 1) \tan \beta. \tag{2}$$

In the above equations

- Φ is the velocity potential,
- σ is the radial frequency,
- l_n is the wave number,
- n is the mode number,
- L_n is the Laguerre polynomial of order n ,
- α_n is the complex modal amplitude,

(x, y) are the offshore/alongshore coordinates and \Re denotes the real part.

These shallow-water solutions are valid for low modes where $(2n + 1) \tan \beta \ll 1$ and are appropriate for the modes and beach slope to be discussed further (Guza and Davis, 1974).

The leaky modes, including incident and reflected waves, form a continuum of modes in (σ, k) space. The velocity potential and deepwater dispersion relation are given approximately by

$$\begin{aligned} \Phi_i &= \Re \{ g\sigma^{-1} (J_0(x), iY_0(x)) \alpha_i e^{i(l y + \sigma t)} \}, \\ \Phi_r &= \Re \{ g\sigma^{-1} (J_0(x), -iY_0(x)) \alpha_r e^{i(l y + \sigma t)} \}, \end{aligned} \tag{3}$$

and

$$\sigma^2 = g|K| \tanh |K|h, \tag{4}$$

where J_0, Y_0 are the zeroth order Bessel functions, subscripts (i,r) denote incident and reflected waves, h is the water depth, and K is the vector wavenumber. These solutions are valid when $\sin \delta \tan \beta$ is small, where δ is the angle of incidence (Guza and Bowen, 1975).

The higher mode edge waves and the leaky modes are quite similar in structure. This, along with the large number of possible modes, complicates observational studies seeking to identify modes. An array capable of separating motions due to many similar modes would be prohibitively large. In addition the modes are likely to be coupled. The modes may arise from a common forcing, or from coherent forcing functions, and the total response must satisfy external boundary conditions. Thus it is likely that the modes are coherent or phase-locked, i.e. $\langle \alpha_n \alpha_m^* \rangle \neq 0$ (where * denotes the complex conjugate and $\langle \rangle$ denotes time averaging).

The modal structure of the infragravity field and the degree of modal coupling are important parameters in models of generation of beach morphology (Holman and Bowen, 1982). A detailed description of the modal response to forcing will also contribute to improved understanding of the dynamics of the nearshore. The large number of possible modes and the potential for coupled modes requires special treatment of observations made in the nearshore. We shall describe and apply a method which utilizes observations from a variety of sensor types and locations, and which explicitly considers modal coupling. Additionally the method may be used to address the relationship between the estimated modal response and observed forcing variables.

Previous investigators have shown that the bulk of observed infragravity energy may be described by free wave modes. Oltman-Shay and Guza (1987) applied maximum-likelihood 2-D spectral estimators to data collected on California beaches during the NSTS study. The method employed utilized only a single observed variable from sensors located along a shore parallel line. Additionally the method assumes the modes are random in phase. The results of the analysis showed that much of the observed energy fell along edge wave modal dispersion lines. The modal structure of the field, as suggested by this method, varied dramatically depending on the variable type (alongshore or cross-shore velocity) subjected to the analysis. This is consistent with the observation that higher modes (and leaky modes) have a relatively large cross-shore velocity component.

Huntley (1988) examined the same data using a qualitative method to assess the importance of modal coupling. He found strong evidence that, over the period of the observations, modes present were coupled. This coupling was associated with alongshore inhomogeneity in the observed velocity field. No quantitative assessment of the modal coupling or relative phases between modes was possible.

We shall present a method which allows simultaneous incorporation of a variety of variables from any sensor location. The method also explicitly estimates the coupling and relative phases of the modes modelled. We shall briefly discuss how measured indices of the forcing might be included to yield estimates of the gain between the forcing and the modal response as modelled.

The Method of Analysis

The observations will be modelled as the resultant of a linear superposition of modes at a single frequency, σ_0 . The observations from the i^{th} sensor, $\theta_i(t)$, are given by

$$\theta_i(t) = \alpha_j(t) f(\phi_{ij}(x, y) \exp i(\ell_j y_i + \sigma_0 t)) + \epsilon_i(t) \quad (5)$$

where i denotes the i^{th} sensor and j the j^{th} mode and $j_{max} < i_{max}$. $\epsilon_i(t)$ is the error term at the i^{th} sensor which may contain unmodelled spatially coherent motions. The function $f(\cdot)$ depends on the sensor location and the variable type. The model is complex and $\theta_i(t)$ may be thought of as the complex demodulate of the observed series at σ_0 .

The model equation may be written in vector form as

$$\underline{\theta} = \mathbf{E}\underline{\alpha} + \underline{\epsilon} \quad (6)$$

where \mathbf{E} is the matrix of modal coefficients and $E_{i,j}$ defines the j^{th} mode at the i^{th} sensor. The cross-spectral matrix of observations, $\langle \underline{\theta} \underline{\theta}'^* \rangle$, (where $'$ is the transpose) at frequency σ_0 is given in terms of the cross-spectral matrix of modal amplitudes by

$$\langle \underline{\theta} \underline{\theta}'^* \rangle = \mathbf{E} \langle \underline{\alpha} \underline{\alpha}'^* \rangle \mathbf{E}' + \text{errors.} \tag{7}$$

It has been shown (Haines *et al.*, in prep.) that the least squares estimate of $\langle \underline{\alpha} \underline{\alpha}'^* \rangle$ is given by

$$\langle \widehat{\underline{\alpha} \underline{\alpha}'^*} \rangle = (\mathbf{E}'^* \mathbf{E})^{-1} \mathbf{E}'^* \langle \underline{\theta} \underline{\theta}'^* \rangle \mathbf{E} (\mathbf{E}'^* \mathbf{E})^{-1}. \tag{8}$$

The quantity minimised is the squared error between the predicted and observed series, summed over the entire cross-spectral matrix. This formulation guarantees that the predicted cross-spectral matrix and the cross-spectral matrix of modal amplitudes are physically realizable and so may be interpreted as cross-spectral matrices. This provides estimates of modal power, coherences and relative phases. As the solution is a linear transformation of the cross-spectral matrix of observations, significance levels follow from standard formulae.

The method may be simply understood by solving (6) in the time domain. The least squares solution gives

$$\hat{\underline{a}} = (\mathbf{E}'^* \mathbf{E})^{-1} \mathbf{E}'^* \underline{\theta}. \tag{9}$$

Squaring and averaging, or forming $\langle \hat{\underline{a}} \hat{\underline{a}}'^* \rangle$, returns (8). Similarly from (9) we may define a cross-spectral matrix of residuals given by

$$\begin{aligned} \langle \underline{\epsilon} \underline{\epsilon}'^* \rangle &= \langle \underline{\theta} \underline{\theta}'^* \rangle + \mathbf{E} (\mathbf{E}'^* \mathbf{E})^{-1} \mathbf{E}'^* \langle \underline{\theta} \underline{\theta}'^* \rangle \mathbf{E} (\mathbf{E}'^* \mathbf{E})^{-1} \mathbf{E}'^* \\ &\quad - \mathbf{E} (\mathbf{E}'^* \mathbf{E})^{-1} \mathbf{E}'^* \langle \underline{\theta} \underline{\theta}'^* \rangle - \langle \underline{\theta} \underline{\theta}'^* \rangle \mathbf{E} (\mathbf{E}'^* \mathbf{E})^{-1} \mathbf{E}'^*. \end{aligned} \tag{10}$$

This matrix is also physically realizable. Decomposition of the cross-spectral matrix of residuals will indicate whether spatially coherent motions remain which are not adequately described by the model fitted.

In practice the sensor array may be incapable of resolving the wide range of modes possible. The model must be limited to those modes which are well resolved. The degree to which modes modelled are resolved is indicated by the condition of the matrix $(\mathbf{E}'^* \mathbf{E})$, where the condition is the ratio of the smallest to largest eigenvalues of the matrix. This provides a useful tool for array design as the matrix may be formed, for given topography and frequency, prior to collecting data. The resolution of the array will vary with frequency as the modal shapes vary and frequency dependent models may be necessary. As a general rule of thumb the condition of the model matrix should exceed the estimated noise to signal ratio of the array.

The incorporation of a variety of sensors may necessitate weighting of the model. This will prevent single energetic observations from dominating the fit. The most straightforward approach is to weight the model by the standard deviation of the observations.

The modelling may also be extended to include forcing variables. In such a case the observed forcing time series are included as observation series and simply passed through the fitting step. The forcing series, $F(t)$, are modelled as

$$F_i(t) = E_{i,j} \alpha_n(t) + 0, \tag{11}$$

where $E_{i,j} = 1$ when $j = n$ and 0 otherwise. The result is that $F_i = \alpha_n$, and the final fitted cross-spectral matrix includes terms of the form $\langle F_i \alpha_m^* \rangle$.

Application

The method of analysis described has been applied to a single data run from the NSTS experiment. Measurements were made at Torrey Pines beach, San Diego in November of 1978. Torrey Pines is a 3 km long beach with slope approximately .02 below MSL. The incident wave field is directionally restricted by offshore islands and for the November 21 run examined 17 two-component Marsh-McBirney flowmeters were deployed. The data were sampled at 64 Hz , low-pass filtered and reduced to 2 Hz . The cross-spectral estimates have a bandwidth of $.00049\text{ Hz}$ giving 10 degrees of freedom. The incident wave field was characterised by a peak frequency of $.067\text{ Hz}$ and a significant wave height of $.86\text{ m}$ (Guza and Thornton, 1985). The cross-spectral matrix is modelled as described and the results averaged across frequency to increase the degrees of freedom. This allows us to model the variation in modal shapes with frequency rather than averaging prior to fitting.

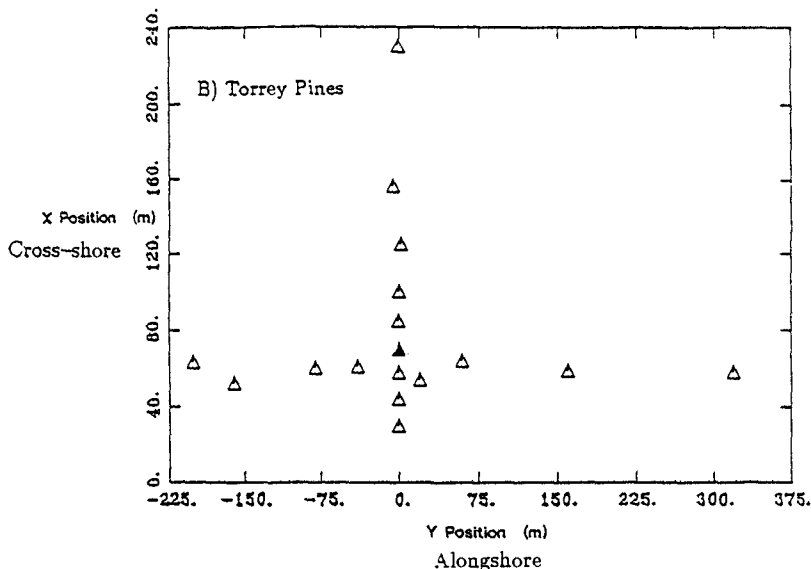


Figure 1. Configuration of flowmeters used in analysis. Symbols indicate position of Marsh-McBirney electromagnetic flowmeters. Shoreline is lower horizontal axis.

The array configuration is shown in Figure 1. The studies previously discussed (Oltman Shay and Guza, 1987, Huntley, 1988) used only the alongshore transect and treated the two velocity components separately. We simultaneously model all the available data. This is particularly helpful in avoiding the spectral gaps caused when an offshore position sees a node in a measured variable. Given the large number of modes possible, some care was taken in choosing a model, as the results of Oltman-Shay and Guza (1987) suggested a wide range of modes were present during the study. However, it is necessary to fit a restricted number of modes which will be representative of the entire field. After a number of trials we chose to fit edge wave modes 0,1,2,4 and 7 (progressive in either direction) and an incident and reflected pair. We chose to fit the same model across all frequencies in order to identify the frequency dependence of the modal field. At any particular frequency simpler models

are as efficient at describing the data - but the complete model is superior across the entire frequency range.

The success of the model in describing the observations is shown in Figure 2. Across most of the range the bulk of the variance and the spectral peaks are well described. The more energetic alongshore velocities are better described than the cross-shore velocities, though the residual variance for the two sensor types is comparable. At low frequencies the model fails to describe the motions present. It is clear that no simple edge wave model will fit these motions. Eigenvector analysis of the cross-spectral matrix of residuals shows that the bulk of the unexplained variance is spatially coherent. This indicates that coherent motions incompatible with edge/leaky wave models are present.

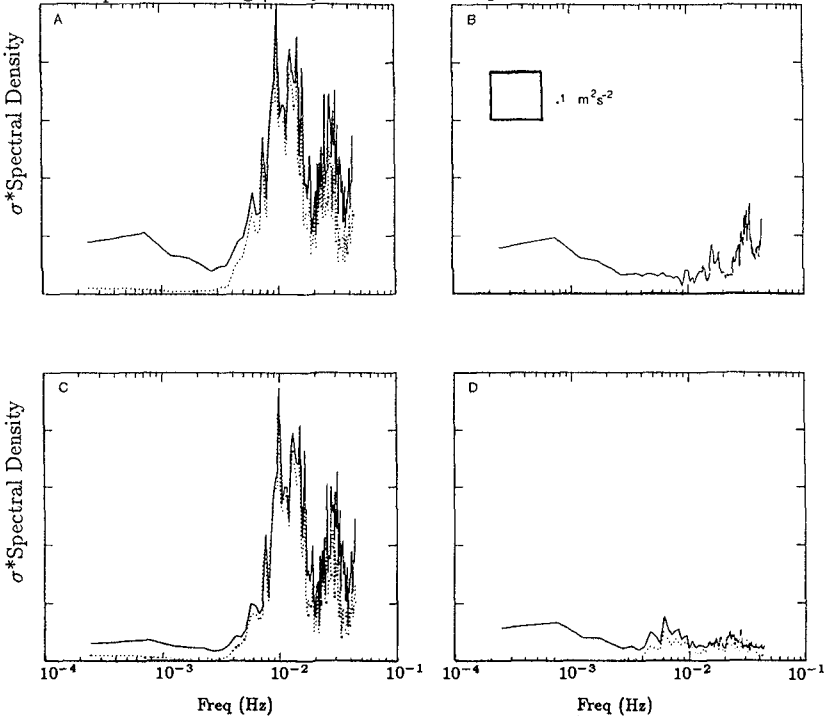


Figure 2. Integrated variance measured (—) and predicted (- - -). Variance is integrated across a) the total array, c) the cross-shore velocity sensors and d) the alongshore velocity sensors. Panel b) shows the total residual variance.

As a rough but independent check of the results Figure 3 shows the predicted shoreline run-up for the model fitted. Measured run-up (Guza and Thornton, 1985) is also shown. The predicted run-up has been calculated by assuming that a standing wave of twice the reflected wave amplitude is seen at the shoreline in addition to the edge waves. Given the limitations of this model and the significant residual energy the agreement is encouraging. Figure 4 shows the predicted run-up for a number of alongshore positions. The substantial variation shows that the degree of modal coupling found is important. It also points out the dangers of assuming spatial homogeneity and the advantages of having shoreline data to verify and constrain modelling techniques.

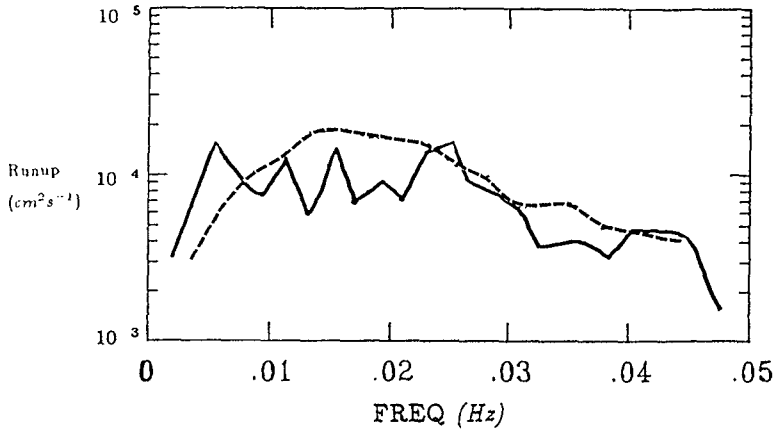


Figure 3. Measured (—) and predicted (---) shoreline run-up spectra at Torrey Pines.

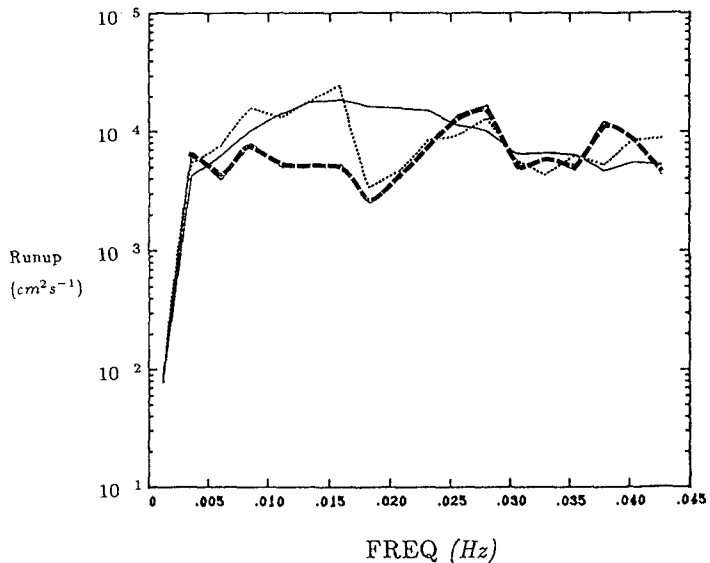


Figure 4. Predicted run-up spectra at Torrey Pines at $y = 0$ (—), $y = 250$ (· · ·) and $y = 500$ (---).

The predicted run-up spectra clearly suggest that the wave field is inhomogeneous. This has important implications for sediment transport and beach profile modelling. In particular it validates the modelling assumptions of Holman and Bowen (1982) that phase-locked modes are important.

The estimated modal amplitude spectra are shown in Figure 5. All modes show negligible amplitude at the lowest frequency. With the possible exception of mode zero, all modes

show enhanced modal amplitudes around $.015Hz$. Modes higher than mode zero show a second peak between $.025$ and $.030Hz$. There is a tendency for northward progressive waves (dotted lines) to be slightly larger, the greatest differences appearing in the neighbourhood of the spectral peaks. Above $.025Hz$ mode zero is forced to small amplitudes as it decays inshore of the array. In general the modal amplitude spectra indicate:

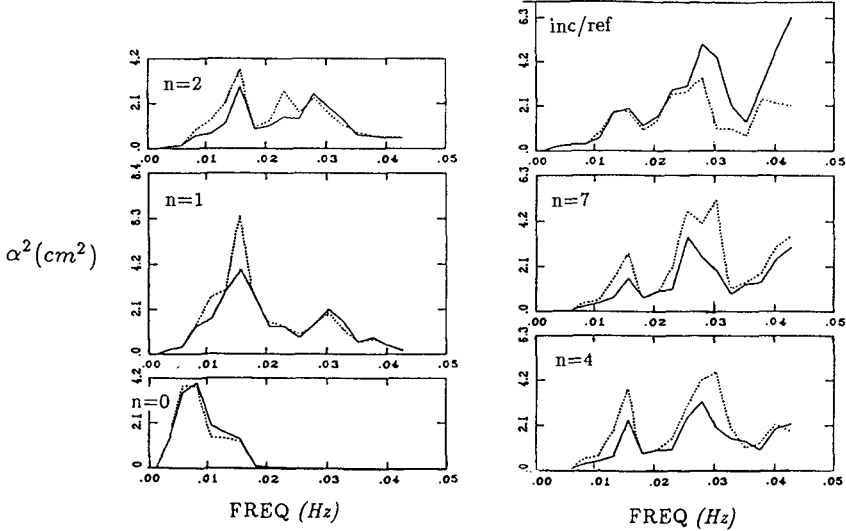


Figure 5. Shoreline amplitude spectra for modes fitted. Mode numbers are indicated in upper left hand corner of spectral plots. Solid (dashed) lines indicate positive (negative) alongshore progression for edge waves and the incident (reflected) wave in the upper right hand panel.

- 1) A wide range of modes, including high modes and leaky waves are present.
- 2) The two directions of edge wave propagation show roughly equivalent amplitudes, with a slight enhancement of the northward propagating waves.
- 3) There are two distinct peaks in the amplitude spectra. The peaks are present for all modes higher than zero. This frequency structure is also seen in the incident and reflected waves.
- 4) Modes higher than two show evidence of increasing amplitude above $.035Hz$.
- 5) The higher frequency peak, $\sim .025 - .030Hz$, is dominated by higher modes with amplitude increasing with mode number.
- 6) The incident wave amplitude increases sharply at the upper frequency limit, and the incident wave is uniformly larger than the reflected wave.

Figures 6 and 7 show the gain and phase for the mode zero and incident and reflected wave pairs. Significantly non-zero gain is equivalent to significantly non-zero modal coupling. The mode zero pair shows significant coupling over a wide range of frequencies, although primarily outside the energetic region of the amplitude spectra. Phase shows no obvious σ^2 dependence which would indicate the presence of an alongshore reflector. The incident/reflected pair also shows significant coupling with the gain less than 1 and generally decreasing with frequency. This frequency dependence of the reflection coefficient has been

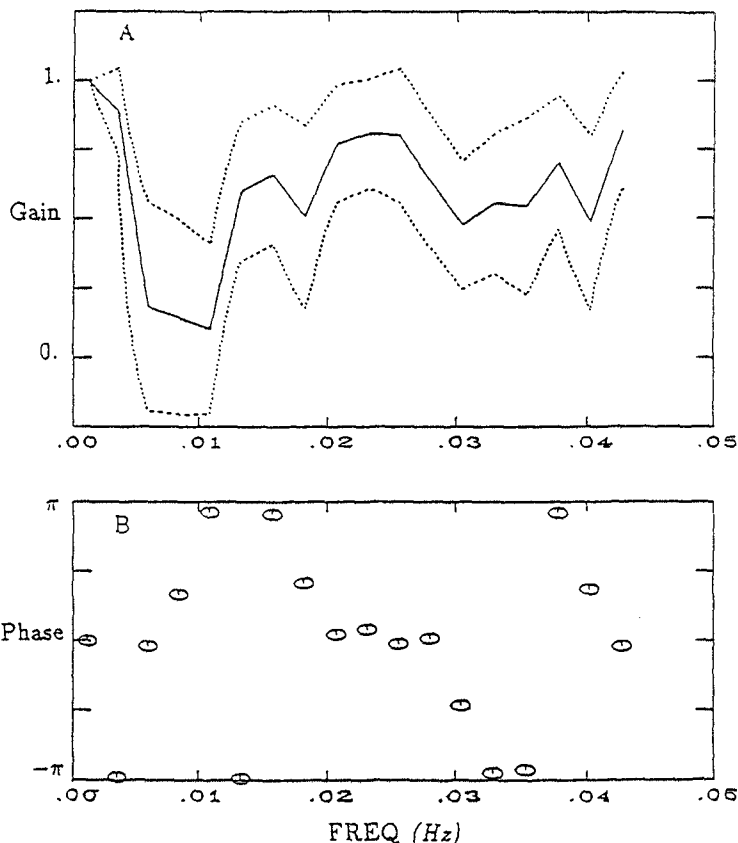


Figure 6. Gain, a), and phase, b), between oppositely progressing mode zero edge waves. Dashed lines on gain plot are upper and lower 95% confidence levels (Jenkins and Watts, 1968).

suggested by a number of authors (Elgar, 1985). The pronounced, quasi-linear trend to the phase is unexplained. Because the incident and reflected waves are largely nondispersive at these frequencies, a linear phase shift may suggest that the cross-shore origin is misplaced, i.e. reflection is occurring away from the shoreline. Determination of this reflection point would require a physical model for the process being described. Phase differences may also be attributable to nonlinearities in run-up or the effects of a porous beach face. These introduce what are presumably higher order modifications to the modelled waves.

Significant squared coherences are shown in Table 1 for all modal combinations at selected frequencies. The occurrence of significant coherences is substantially greater than that expected for a system composed of noise. Apart from a slight tendency for higher modes to be coupled to the incident wave, there appear to be no particular pairs which exhibit consistently high coupling. Significant coupling also seems unrelated to modal amplitude

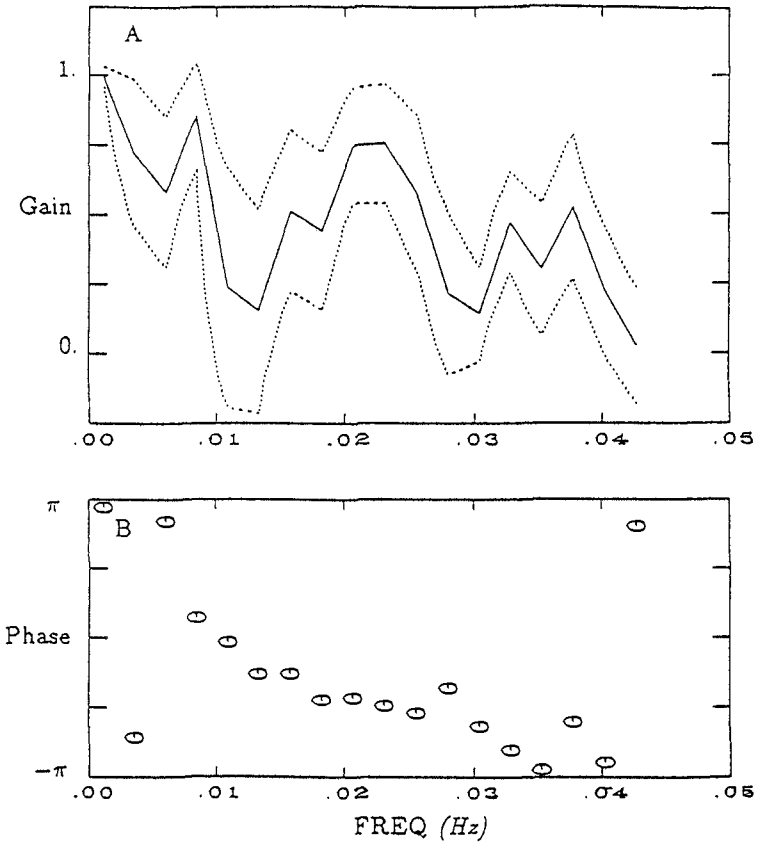


Figure 7. Gain, a), and phase, b), between incident and reflected waves. Dashed lines on gain plot are upper and lower 95% confidence intervals (Jenkins and Watts, 1968).

or frequency.

Conclusions: We have presented and applied a method of extracting modal information from observed dynamic variables. The method uses all available data and explicitly considers phase-locking of modes. The method may be extended to include forcing variables.

The data set examined comprised an unusually large sensor array. Even so it is not possible to consider all the modes which might be expected to be present. The results of the

Table 1
Modal Coupling - Torrey Pines

	0 ⁺	0 ⁻	1 ⁺	1 ⁻	2 ⁺	2 ⁻	4 ⁺	4 ⁻	7 ⁺	7 ⁻	I	R
0 ⁺	-	-	.65	.14	.32	.26	-	.27	-	.21	.20	.20
0 ⁻		-	.18	.69	.30	.36	.27	-	.19	-	-	-
1 ⁺			-	.38	.87	.29	.55	-	.33	-	-	-
1 ⁻				-	.28	.88	-	.58	-	.36	-	-
2 ⁺					-	.12	.87	-	.67	-	.13	-
2 ⁻						-	-	.88	-	.69	-	-
4 ⁺	$\sigma = .0061Hz$						-	-	.94	.25	.24	-
4 ⁻								-	.25	.95	.23	.21
7 ⁺									-	.47	.31	.19
7 ⁻										-	.31	.26
I											-	.38
R												-
	0 ⁺	0 ⁻	1 ⁺	1 ⁻	2 ⁺	2 ⁻	4 ⁺	4 ⁻	7 ⁺	7 ⁻	I	R
0 ⁺	-	.43	-	-	-	-	-	-	-	-	-	-
0 ⁻		-	-	-	-	-	-	-	-	-	-	-
1 ⁺			-	.18	.45	-	-	-	.19	-	.14	.20
1 ⁻				-	-	.40	-	-	-	-	-	-
2 ⁺					-	-	.45	.25	-	.27	-	-
2 ⁻						-	-	.73	-	.49	-	.12
4 ⁺	$\sigma = .0134Hz$						-	-	.77	-	-	.13
4 ⁻								-	-	.93	.36	.32
7 ⁺									-	.22	.32	.38
7 ⁻										-	.47	.44
I											-	-
R												-
	0 ⁺	0 ⁻	1 ⁺	1 ⁻	2 ⁺	2 ⁻	4 ⁺	4 ⁻	7 ⁺	7 ⁻	I	R
0 ⁺	-	.64	-	-	-	.14	-	.19	.26	.49	.76	.76
0 ⁻		-	-	-	-	-	.25	-	.49	.25	.75	.76
1 ⁺			-	-	-	-	-	-	-	-	-	-
1 ⁻				-	-	-	-	-	-	-	-	-
2 ⁺					-	-	.37	-	-	-	-	-
2 ⁻						-	-	.47	-	.14	-	-
4 ⁺	$\sigma = .0208Hz$						-	-	.74	.12	.19	.19
4 ⁻								-	-	.74	.19	.16
7 ⁺									-	.13	.49	.39
7 ⁻										-	.46	.48
I											-	.63
R												-

Table 1 The coherence squared between modes. Significant values of coherence squared (Jenkins and Watts, 1968) are shown for all modal pairs. +/- indicates a wave progressing northward/southward.

Table 1 - continued
 Modal Coupling - Torrey Pines

	0 ⁺	0 ⁻	1 ⁺	1 ⁻	2 ⁺	2 ⁻	4 ⁺	4 ⁻	7 ⁺	7 ⁻	I	R
0 ⁺	-	.49	-	.13	-	.14	.19	.40	-	.14	.45	.16
0 ⁻		-	.13	-	-	-	.24	.36	-	-	.38	.20
1 ⁺			-	-	-	-	-	.17	-	-	-	-
1 ⁻				-	-	-	-	-	-	-	-	-
2 ⁺					-	-	.19	-	.12	.26	-	-
2 ⁻						-	-	-	.13	-	-	-
4 ⁺	$\sigma = .0281Hz$						-	.12	.30	.13	.25	-
4 ⁻								-	.15	.39	-	.25
7 ⁺									-	.55	-	-
7 ⁻										-	.13	.18
I											-	-
R												-
	0 ⁺	0 ⁻	1 ⁺	1 ⁻	2 ⁺	2 ⁻	4 ⁺	4 ⁻	7 ⁺	7 ⁻	I	R
0 ⁺	-	.28	.83	.38	.12	-	-	-	-	-	-	-
0 ⁻		-	.30	.77	-	.15	-	.13	-	-	.15	-
1 ⁺			-	.43	-	-	-	-	-	-	-	-
1 ⁻				-	-	-	-	-	-	-	-	-
2 ⁺					-	-	-	-	-	-	-	-
2 ⁻						-	-	-	-	-	-	-
4 ⁺	$\sigma = .0354Hz$						-	-	-	.13	.25	.20
4 ⁻								-	-	-	.27	-
7 ⁺									-	.38	.19	-
7 ⁻										-	.14	-
I											-	.18
R												-
	0 ⁺	0 ⁻	1 ⁺	1 ⁻	2 ⁺	2 ⁻	4 ⁺	4 ⁻	7 ⁺	7 ⁻	I	R
0 ⁺	-	.67	.92	.55	-	-	-	-	.21	.32	.53	.22
0 ⁻		-	.80	.90	-	-	.15	-	.24	.14	.57	.18
1 ⁺			-	.45	.12	-	-	-	.73	.37	.52	.25
1 ⁻				-	-	-	.12	-	.25	.17	.69	.14
2 ⁺					-	-	-	-	-	-	-	-
2 ⁻						-	-	.14	-	-	-	-
4 ⁺	$\sigma = .0427Hz$						-	.14	.23	-	-	-
4 ⁻								-	-	-	-	-
7 ⁺									-	-	.15	-
7 ⁻										-	.30	-
I											-	-
R												-

Table 1 The coherence squared between modes. Significant values of coherence squared (Jenkins and Watts, 1968) are shown for all modal pairs. +/- indicates a wave progressing northward/southward.

fit suggest a variety of modes are present and that significant phase-locking occurs. This has important implications for sediment transport, beach morphology and the modelling of edge wave dynamics.

References

- Bowen, A.J., and D.L. Inman, Edge waves and crescentic bars, *J. Geophys. Res.*, 76, 862-8671, 1971.
- Bowen, A.J., and D.A. Huntley, Waves, long waves and nearshore morphology, *Marine Geology*, 60, 1-13, 1984.
- Eckart, C., Surface waves in water of variable depth. Wave report, SIO Ref. 51-12, Scripps Inst. Oceanogr., La Jolla, CA, 99pp, 1951.
- Elgar, S., Shoaling surface gravity waves, Ph.D. thesis, Scripps Inst. Oceanogr., La Jolla, CA 123 pp., 1985.
- Guza, R.T., and R.E. Davis, Excitation of edge waves by waves incident on a beach, *J. Geophys. Res.*, 79, 1285-1292, 1974.
- Guza, R.T., and A.J. Bowen, Finite amplitude edge waves, *J. Mar. Res.*, 34, 269-293, 1976.
- Guza, R.T., and Inman, D.L., Edge waves and beach cusps, *J. Geophys. Res.*, 80, 2997-3012.
- Guza, R.T., and E.B. Thornton, Observations of surf beat, *J. Geophys. Res.*, 80, 2997-3172, 1985.
- Haines, J.W., K.R. Thompson, and D. Wiens, Fitting dynamical modes to data. (in prep.)
- Holman, R.A., and A.J. Bowen, Bars, bumps and holes: models for the generation of complex beach topography, *J. Geophys. Res.*, 87, 457-468, 1982.
- Holman, R.A., and A.J. Bowen, Longshore structure of infragravity wave motions, *J. Geophys. Res.*, 89, 6446-6452, 1984.
- Huntley, D.A., Evidence for phase-coupling between edge wave modes, (in prep.)
- Jenkins, G.M., and D.G. Watts, Spectral analysis and its applications, Holden-Day, Oakland, CA, 525 pp., 1968
- Oltman-Shay, J., and R.T. Guza, Infragravity edge wave observations on two California beaches, *J. Phys. Oceanogr.*, 17, 644-663, 1987.
- Symonds, G., D.A. Huntley and A.J. Bowen, Two-dimensional surf beat, long wave generation by a time-varying breakpoint, *J. Geophys. Res.*, 87, 492-498, 1982.